Journal Title: Image and vision computing.
Vol: 18 **No:** 13
Date: 2000

Pages: 1025-1032

Article Author: Soille
Article Title: Morphological image analysis applied to crop field mapping

Image and Vision Computing 18 (2000) 1025–1032

www.elsevier.com/locate/imavis

Morphological image analysis applied to crop field mapping

P. Soille*

Image Analysis and Control Group, BBSRC-Silsoe Research Institute, Wrest Park, Silsoe, Beds MK45 4HS, UK

Received 28 October 1999; revised 13 March 2000; accepted 31 March 2000

Abstract

Previous research about automatic vision systems applied to crop field imaging fails when the scene is too complex, in the sense that the individual plants are connected together or to weed patches. In this paper, we show that morphological image processing can efficiently solve these problems provided that a priori knowledge about the shape of the plants is available. For example, vein networks appearing within the target plant leaves allow us to automatically mark and segment the plants. Results are shown on a series of outdoor scenes of a test field.

Keywords: Image analysis; Pattern recognition; Mathematical morphology; Clustering; Colour; Image processing chain; Application

1. Motivation

Some agricultural tasks performed in a crop field consist of applying chemical treatment to the plants or mechanically removing the weeds. Previous research has shown that a vision system mounted on an autonomous vehicle can perform these tasks automatically [1–3]. For navigation purposes, the vehicle does not need the full outline of the plants, but rather the positioning of their centre (under the reasonable assumption that the plants have been planted in a row). Techniques such as a modified Hough transform [4] or structure from motion [1] have proven to be successful for locating the plant rows or centres. These techniques require a rough segmentation producing a binary image marking the plants. This is usually achieved by acquiring first a near infrared (NIR) image because vegetation has a significantly higher reflectance than soil for wavelengths around 800 nm under natural daylight (direct or diffuse). A global threshold of the NIR image outputs therefore a reasonably good map of soil and vegetation ground covers [5,6]. Plants and weeds are then separated using, among other assumptions, a size criterion (connected components corresponding to plants have a larger area than those corresponding to weeds) and a topological constraint (plants are defined by single blobs which do not touch each other nor are connected with weeds). Our research was therefore motivated by the need for a technique that allows the recognition of plants in situations where these hypotheses are not acceptable. We show that it can be achieved by applying a series of mathematical morphology [7–10] transformations on an input true colour image of the scene. Size and topological constraints have been suppressed and replaced by a priori knowledge concerning the morphology of the plant.

The paper is organised as follows. After a short description of the image characteristics, Section 2 presents the non-parametric classification technique used for segregating soil and vegetation pixels. Section 3 describes the algorithm developed for extracting an estimate of the plant position. The extraction of the outline of the plants is detailed in Section 4. Before concluding, Section 5 discusses results obtained on a database of outdoor scenes.

2. Soil and vegetation classification

During a test-phase, we acquired a series of 18 colour images using a camera mounted on a gantry so as to acquire vertical views of an experimental field. The colour negatives were digitised at a resolution similar to that produced by the RGB digital colour CCD camera that we plan to equip the autonomous vehicle with. In addition, other tests at various resolutions can be performed on the same scene by scanning the negatives at various resolutions. A typical image is shown in Fig. 1. Compared to NIR images, the colour images have a much higher spatial information content. Indeed, the within plant reflectance variations in the visible wavelengths are much higher than that in the NIR. In

* Present address: EC Joint Research Centre, Space Applications Institute, TP 441, I-21020 Ispra, Italy. URL: http://ams.egeo.sai.jrc.it/soille. Tel.: +39-0332-785-068; fax: +39-0332-789-536.

E-mail address: pierre.soille@jrc.it (P. Soille).

0262-8856/00/$ - see front matter
PII: S0262-8856(00)00043-3

Fig. 1. Typical 369 × 369 true RGB colour image of a test field showing soil, overlapping plants, and weeds.

particular, the veins appearing in the plants of Fig. 1 are hardly visible in the corresponding NIR image, see for example Ref. [4, Fig. 1].

On the other hand, contrary to the NIR-images, a global threshold of a single colour component of the original RGB image cannot be used for discriminating between the vegetation and the soil. Indeed, from the red–green feature space shown in Fig. 2(a), it can be seen that it is necessary to use both spectral components for discriminating soil from vegetation because there is a lack of separability in either original band (also occurring when considering the blue band). Using the principal component would not be sufficient either as it is not the overall variance that would need to be maximised for separating the clusters but rather the among category variance (while minimising the within category variance). The canonical analysis implements this idea but it requires the covariance matrices of each class to be known [11]. A simpler approach is to choose a colour transform producing a new colour component allowing for a separation between soil and vegetation. For example, the hue component obtained by transforming the RGB colour space into the HSI (Hue Saturation Intensity) colour space could be considered. However, with natural lighting, at least two problems can occur. Firstly, the same surface component can be illuminated from two sources, each having a different colour, i.e. sunlight (in direct sun) and skylight (in shadows). Thus the hue will be different for the same surface [12]. A second problem occurs with highlights that are, from the dichromatic reflection model, a mixture of the body and the illuminant colour. Thus pixels from plant surfaces, which have the mixture in different proportions, will not necessarily form clear clusters in a one-dimensional feature space obtained by a simple colour space transform. They will however form clusters in a higher dimensional space [13]. In addition, the one-dimensional approach would also fail separating additional clusters occurring for other plants such as those encountered in horticulture due to the presence of inflorescences. There is therefore a need for considering a more general approach suited to the processing of two- or even three-dimensional feature spaces. We propose to use the non-parametric morphological classification technique described in Refs. [14, 10, chap. 10]. It consists of a watershed-based clustering, assuming that the searched clusters appear as peaks in the feature space. This assumption is typical for non-parametric clustering techniques [15, pp. 5–9] such as the iterative growth of an elliptical cluster around the densest points described in Ref. [16].

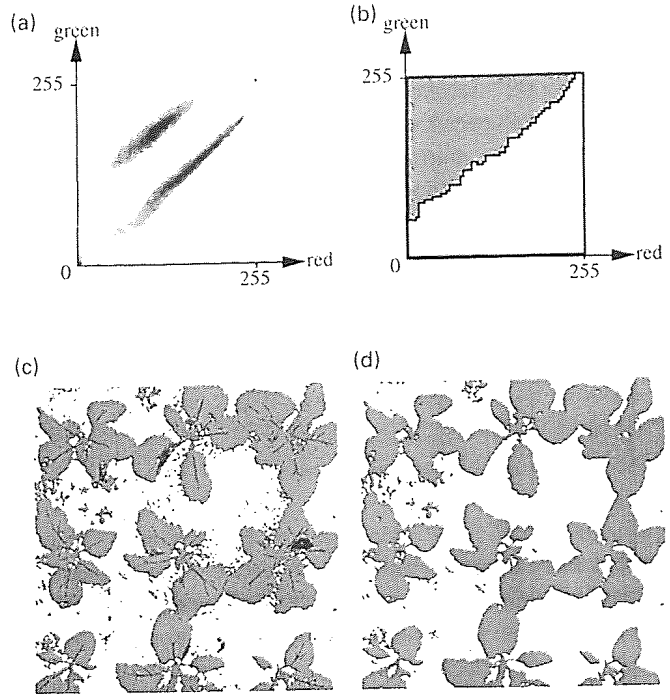

Fig. 2. Morphological unsupervised clustering applied to the red–green feature space of Fig. 1 and resulting classification (see text for a detailed explanation). (a) Green versus red feature space (i.e. bivariate histogram also called scatter plot); (b) Watersheds of filtered feature space; (c) Classification using watershedded feature space as LUT; (d) Final classification using majority rule for assigning the black regions of (c) to either the soil or vegetation categories.

Let us summarise the successive steps of the watershed-based clustering leading to the final classification, starting from the colour image shown on Fig. 1. We need first to compute for each pixel a series of features so as to make each searched category appear as a cluster or peak in the corresponding feature space (in theory, the method applies to n-dimensional feature spaces but in practice it is restricted to a maximum of three dimensions, because processing time and memory requirements are proportional to 256^n, assuming 256 possible values for each feature). Since the input image is a true RGB colour image, three features per pixel are already available. In fact, as already pointed out, the red

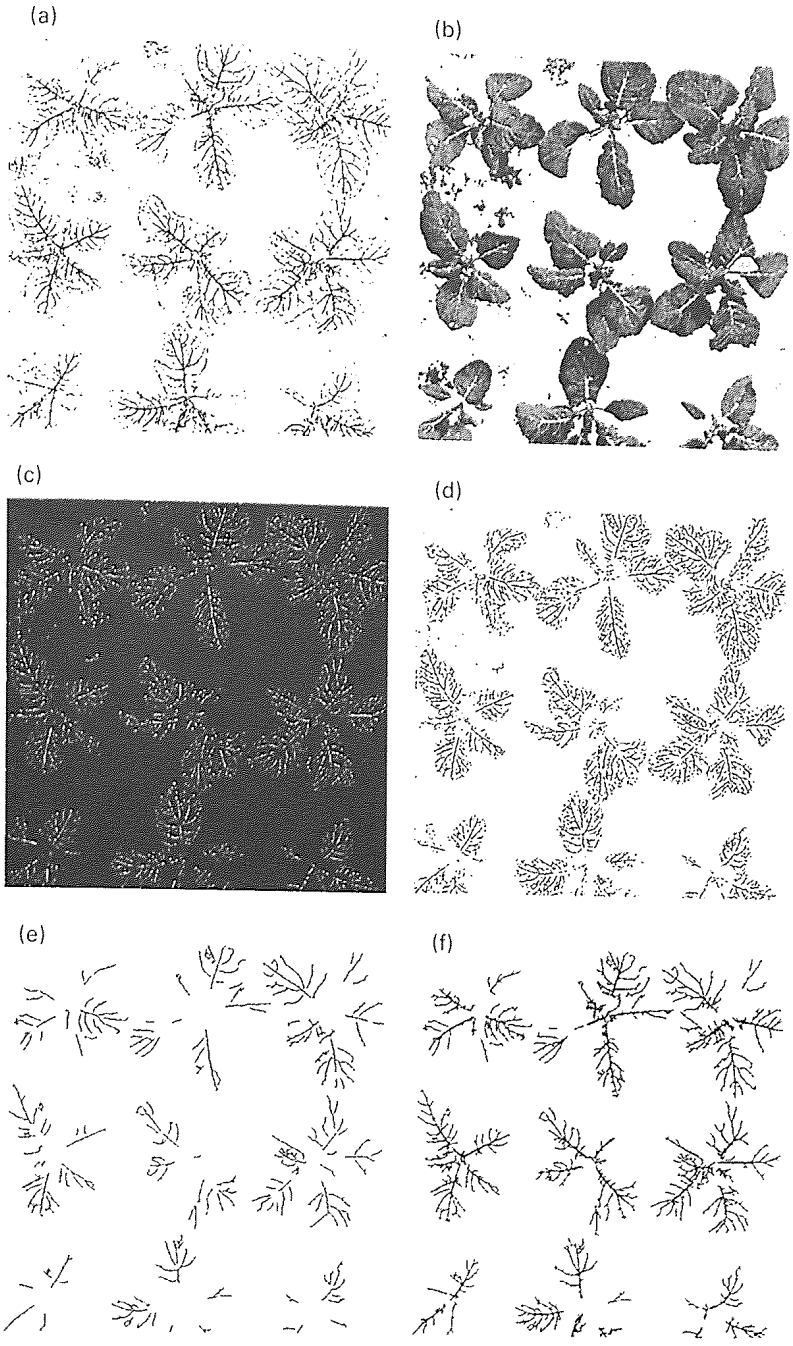

Fig. 3. Vein detection. f is the intensity image of the original colour image using the vegetation class as region of interest (see details in text).(a) Threshold of white top-hat with a 3×3 SE: $T_{[2,255]}[\mathrm{WTH}_{3\times3}(f)]$; (b) Parametric opening: $\gamma_{3\times3,\ 4}(f)$; (c) Top-hat: $\mathrm{WTH}_{3\times3,\ 4}(f) = f - \gamma_{3\times3,\ 4}(f)$; (d) Threshold: $T_{[1,255]}[\mathrm{WTH}_{3\times3,\ 4}(f)]$; (e) Filtered threshold (d); (f) Geodesic reconstruction of (a) $\cup$ (e) from (e).

and green components are sufficient for the purpose of separating the vegetation from the soil pixels. Indeed, two well separated comet-shaped clusters can be observed in the bivariate red–green histogram (scatter plot) displayed in Fig. 2(a): the lower one for the soil and the upper one for the vegetation. The oversegmentation of the feature space that would result from the application of the watershed transformation on the complemented bivariate histogram is avoided by considering the two peaks of highest dynamic [17] as relevant markers (i.e. the flooding simulation will only start from these two markers). The resulting labelled feature space is shown in Fig. 2(b). It is then used as a look-up-table for classifying the pixels of the input image as shown in Fig. 2(c). At this stage, there are three classes: soil, vegetation, and undefined. This latter class corresponds to the watershed line of the feature space plus the boundary of the definition domain of the feature space. This boundary corresponds to the image pixels whose spectral values are falling at both ends of the dynamic range of the sensor in either the green or red component, i.e. the outliers. Indeed, the decision concerning the class of these pixels cannot be made on the basis of their spectral values. We consider therefore the spatial rule assigning each black (undefined) connected component of Fig. 2(c) to the most represented

class of their external boundary pixels (majority rule). The final automatic classification into soil and vegetation categories is shown in Fig. 2(d).

This approach also illustrates that a classification based on spectral attributes only could not be used to discriminate saturated regions within the plants (i.e. parts of the veins) and soil (i.e. the white stones) since they have the same spectral values in all three channels. It is the neighbouring (spatial) information that leads to the correct decision. Depending on the application, other schemes may be considered for integrating spatial information in the watershed-based classification technique as described in Ref. [10].

3. Plant centre positions

In satellite remote sensing applied to ground cover classification, the spectral signature of a pixel is often enough for detecting its category assuming that a series of well chosen spectral bands are available (e.g. 7 bands for Landsat Thematic Mapper). However, at the scale of individual plants, it has been shown in Ref. [18] that even hyperspectral reflectances (150 spectral bands in the range 400–1000 nm) cannot be directly used for reliably discriminating plants from weeds because the reflected light is too much affected by external unknown variables such as soil type, water content, nutrient levels, and diseases [19].

We have therefore decided to restrict the spectral information to the standard RGB channels. The spectral information allows for robust distinction between soil and vegetation as highlighted in Section 2. On the other hand, given the physical nature of the objects we are sensing (mainly soil and vegetation) and the lighting conditions (natural daylight), any channel of the input colour images contains more spatial information content than the NIR images used in previous studies. This opens an avenue for detecting plants using a priori knowledge about their morphology. For a general-purpose algorithm, the required resolution depends on the scale at which discriminant shape features appear for each specific plant that needs to be recognised.

In our test example (also used for the autonomous vehicle prototype), the relatively low resolution of our input images is enough because the plants show a strong feature in the form of a network of veins radiating from their centre. More precisely, veins are thin networks brighter than their background (unless otherwise stated, we only use the intensity channel of the input RGB image and restrict our treatments to the region of interest defined by the vegetation class). Rather than looking for a direct extraction of the veins, their selective suppression can be easily achieved by opening the intensity image with a square structuring element (SE) slightly larger than the largest veins. The veins themselves are then enhanced by computing the arithmetic difference between the original and opened images. This operation is known in morphology as a top-hat by opening [20], also called white top-hat and denoted by WTH. The top-hat is then thresholded[1] for producing the binary image shown in Fig. 3(a).

However, the opening step suppresses not only the veins but also all bright image structures than cannot contain the SE. An elegant solution to this problem is to consider a more selective opening known as rank-max opening [21] or simply parametric opening [10]. Indeed, rather than using a plain discrete SE B whose cardinal number equals n pixels (i.e. $\mathrm{card}(B) = n$), this type of opening consists in unioning the morphological openings by all possible subsets B_i of B containing λ pixels ($1 \leq \lambda \leq n$). For discrete grey scale images, the union operator simply generalises to the point-wise maximum operator $\vee$. We denote by $\gamma_{B,\lambda}$, the parametric opening (rank-max opening) with a SE B and parameter λ:

$$\gamma_{B,\lambda} = \bigvee_i \{\gamma_{B_i} | B_i \subseteq B \text{ and } \mathrm{card}(B_i) = \lambda\}, \quad (1)$$

where $1 \leq \lambda \leq n$ and $n = \mathrm{card}(B)$ Notice that the smaller λ is, the more selective is the corresponding parametric opening. More precisely, the following ordering relationship holds: $\gamma_{B,n} = \gamma_B \leq \gamma_{B,n-1} \leq \cdots \leq \gamma_{B,2} \leq \gamma_{B,1} = I$, where I denotes the identity transform. From a computational point of view, it can be seen that the upper bound for the number of distinct SEs B_i in Eq. (1) equals $n!/\lambda!(n-\lambda)!$. This number is too large for most real applications. Fortunately, it can be shown [9, pp. 201–202] that the rank-max opening is equivalent to the intersection (point-wise minimum operator $\wedge$) between the input image and the dilation by $\check{B}$ of its rank filter ξ using B as kernel and $n - \lambda + 1$ as rank:

$$\gamma_{B,\lambda} = I \wedge (\delta_{\check{B}} \xi_{B,n-\lambda+1}), \quad (2)$$

where $\check{B}$ is the reflected SE of B. A fast algorithm for rank filters based on the moving histogram technique [22] initially introduced for median filters is detailed in Ref. [23].

One pixel thick veins are extracted by computing the white top-hat with a parametric opening by a 3×3 SE and parameter equal to 4. The parametric opening of the intensity image is displayed in Fig. 3(b) and the corresponding top-hat in Fig. 3(c). The top-hat is then thresholded for all values larger than zero (Fig. 3(d)), ensuring thereby that veins are extracted independently of their contrast (no threshold selection required). The resulting binary image is much more suited to the removal of non-vein pixels than the threshold of the raw top-hat. Indeed, the considered parametric opening does not filter out the intersections of the veins. Veins appear therefore mainly as unconnected one pixel thick line segments in the threshold top-hat shown in Fig. 3(d), contrary to the original thresholded

[1] We denote by T_{t_1,t_2} the threshold operator which sets all pixels of the input image in the range $[t_1, t_2]$ to 1 and the others to 0. Note that the definition and notations of all operators used in this paper can be found in Ref. [10].

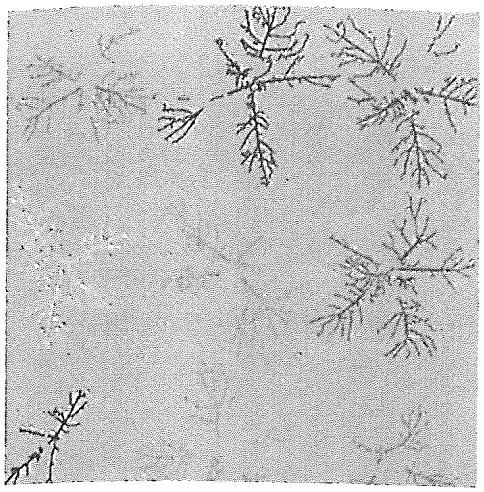

Fig. 4. Hierarchical clustering of the veins shown in Fig. 3(f).

top-hat shown in Fig. 3(a). A combination of a surface area opening [24] on both 4- and 8-connected component is performed to make sure that the remaining components all belong to veins (see Fig. 3(e)). So far, the filter extracts only the 1-pixel thick vein segments. The full network of veins shown in Fig. 3(f) is obtained by using these vein segments as seeds for reconstructing the threshold of the top-hat of the original image by a morphological opening with a plain 3×3 SE (Fig. 3(a)).

The final step consists of clustering the veins belonging to the same plant into a unique cluster. A hierarchical clustering of each connected component of the detected veins produces correct results provided that the pixels are given a weight equal to their grey level in the intensity component of the original colour image. Indeed, pixels closer to the centre of the plants have significantly larger intensity values. The Euclidean distance at which clustering is stopped can be automatically detected since there is a significant gap between the initial merging of the veins belonging to a given plant and the start of merging with those of neighbouring plants. The output of the vein clustering is shown in Fig. 4. By construction, the hierarchical clustering also outputs the centre of each cluster. Their position can then be used for guiding the vehicle [25].

4. Plant outline

The clustered veins provide us with a set of markers roughly marking each individual plant although not indicating the position of the plant outlines. This situation is ideal for region growing procedures since their major challenge consists precisely in determining relevant seeds for initiating the growth process. We show here that the watershed-based region growing technique is suited to the delineation of the plants. This technique not only requires markers for the object one wants to detect but also for their background. The veins mark the plants but we lack of a marker for the weeds.

A solution to this problem is to first compute the watersheds of the segmentation function without markers, i.e. allowing for an oversegmentation, and then reconstruct all catchment basins that are marked by the labelled veins so as to output an image of the segmented plants. We still need to define the segmentation function that will control the flooding procedure, i.e. it has to have high values along the boundaries of the searched objects. The magnitude of a gradient operator fulfils this need. For example, Fig. 5(a) shows the output of the morphological gradient applied to an opening the intensity image. The role of the opening[2] is to remove the veins because otherwise high gradient values would appear within the plants, i.e. at the boundaries of the veins. Fig. 5(b) shows the filtering of the segmentation function using the h-minima transform for a contrast threshold of 20 grey scale levels. This filtering reduces drastically the number of image minima. The watersheds of the resulting segmentation function are shown in Fig. 5(c). All catchment basins that are marked by the clustered veins are then reconstructed so as to output the final outline of the plants (see Figs. 5(d) and (e)).

5. Results and discussion

Results obtained on a series of 15 images are shown in Fig. 6. The a priori knowledge and parameters used in the image processing chain are summarised hereafter for each module while describing the criteria used for selecting the value of each parameter (size values are in pixels):

1. Soil and vegetation classification module:
   - Number of clusters ($n = 2$). This allows us to use the two first peaks of highest dynamic as markers of the feature space before applying the watershed transformation. A fundamental assumption is that the relevant clusters appear as peaks in the feature space.
   - There is no need for other parameters in this module since the classification is non-parametric and automatically adapts to changes in soil and vegetation reflectances (see electronic annexe).
2. Veins extraction module:
   - Width of square SE for white top-hat ($wthsz = 3$). It must be slightly larger than the width of the largest veins.
   - Parameter value for the parametric opening ($\lambda = 4$). Since a 3×3 SE is considered, a parameter value of 4 allows for the extraction of thin nets only (one pixel thick).
   - Two surface area criteria for the filtering of the thresholded top-hat by a parametric opening: Each connected component must contain either at least

[2] It is the same opening as that used for the raw top-hat by opening in Section 3.

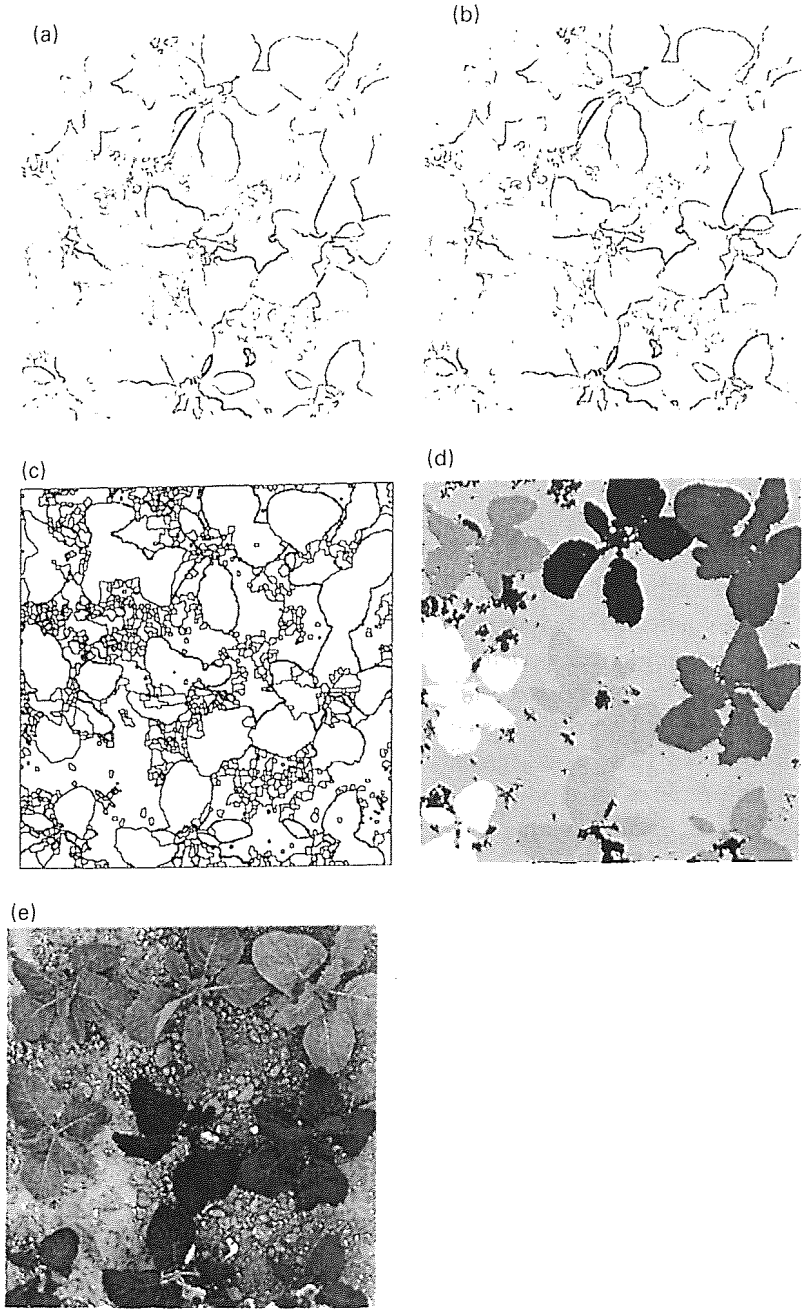

Fig. 5. Watershed-based segmentation of the plants (see text). (a) Morphological gradient of opened intensity image; (b) Segmentation function defined as the h-minima transform of the morphological gradient; (c) Watersheds of the segmentation function (without markers); (d) Reconstruction of the catchment basins marked by the labelled veins (the reconstruction operates in the vegetation class only); (e) Segmented plants overlaid on input image.

$t_1 = 16$ 8-connected pixels or $t_2 = 9$ 4-connected pixels.

- Threshold level for the raw top-hat by opening ($t = 32$). It must enhance the veins while not connecting them with other objects.
- Maximal Euclidean distance for merging two clusters ($d = 50$). It must be smaller than the distance between two plants.

3. Marker-controlled segmentation module:
   - Width of square SE for the morphological gradient ($gradsz = 3$). It depends on sharpness of edges, here an elementary size is enough.
   - Contrast value for h-minima filtering ($h = 20$). It must be chosen so as to merge catchment basins whose dynamic value is less than h.

The same procedure with identical parameter values has been used to produce the results shown in Fig. 6 (see also electronic annexe for all intermediate results). The performance of the algorithm is satisfactory in the sense that (i) all plants fully visible in the image frame are detected, (ii) all connected plants are separated, and (iii) almost no weeds have been detected as plants. Notice that the lack of vein information of few plant leaves has

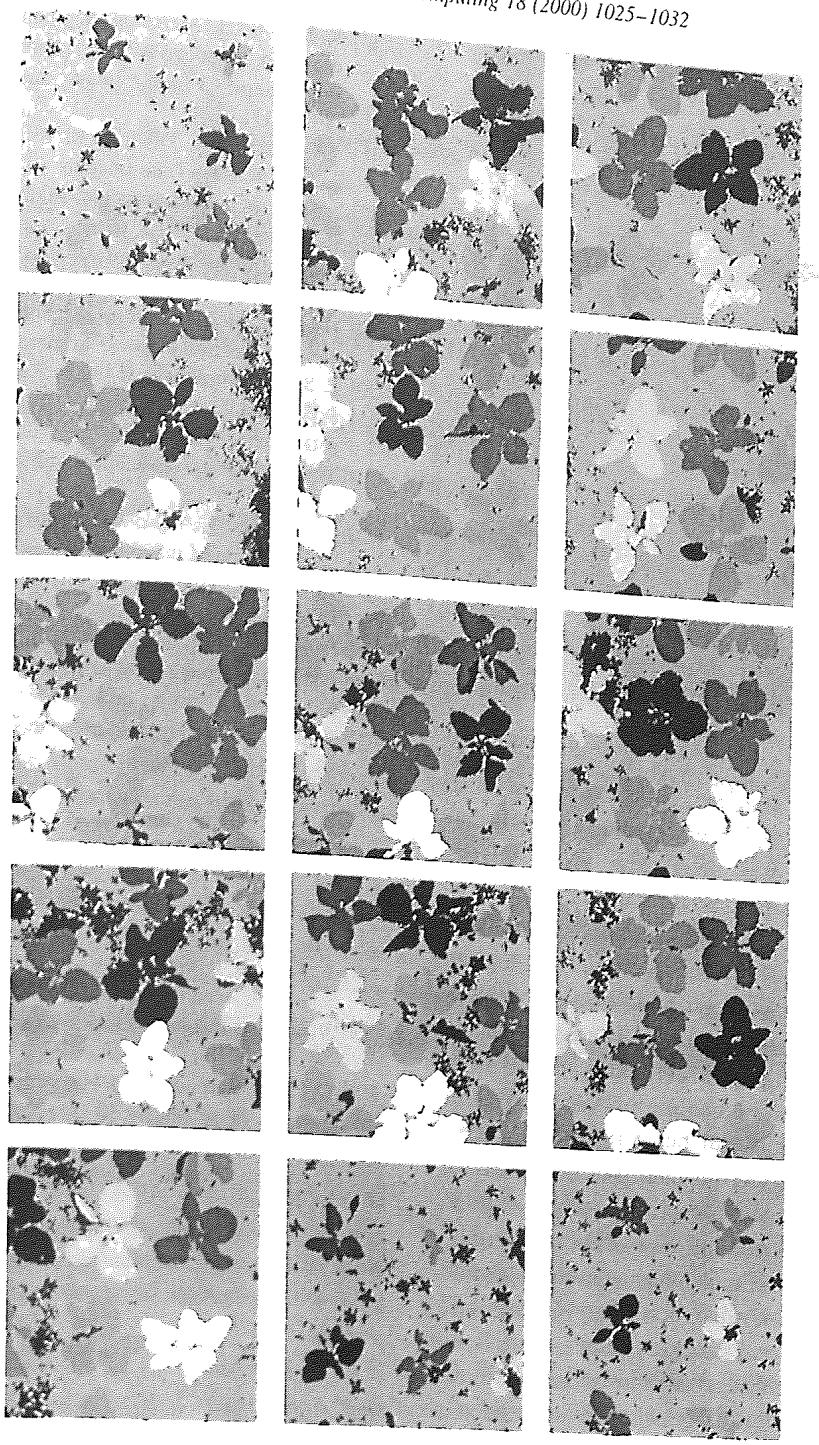

Fig. 6. Results obtained on a series of 15 images showing different growth stages, connections between plants, weed patterns, and natural lighting conditions (labelled detected plants are shown in colour, weeds in black, and soil in grey shade).

hampered their detection (mostly for plants not fully visible in the image frame).

5. Conclusion and perspectives

This application illustrates that morphology is very well suited to problems where a priori knowledge about the scene can be translated into a series of morphological operators. In addition, the resulting image processing chain is controlled at every step so that parameters associated with each step can be tuned without affecting the behaviour of other steps. This makes parameter selection much easier and techniques, such as receiver operator characteristics [26], can be used for automatically selecting the best parameter values in cases where ground truth is available. The proposed modular approach is generic in the sense that it could be adapted for segmenting and classifying other collection of objects presenting discriminant spatial and spectral properties, assuming that foreknowledge about these properties is available and that it can be translated into chains of image processing operators.

Our current research concentrates on the behaviour of the proposed technique against a wider spectrum of plant

Fig. 7. Sampled image scanned at a much higher resolution. At this resolution different weed species can be recognised (five types in the displayed region).

growth rates and weed infestations. Its real-time implementation for use on the autonomous vehicle will then be investigated. At a later stage, we think that an automatic program might translate the taxonomic description of a plant into a series of morphological transformations. The tuning of the program by a non-expert could certainly benefit from research on knowledge-based control of vision systems [27]. Eventually, using additional range information [28], we believe that an automatic system could be used for distinguishing common weeds occurring within a given crop field. The tackling of the corresponding challenging computer vision and pattern recognition problems would be a major achievement towards precision agriculture and selective use of herbicids and other chemicals. This issue will be addressed by processing the same scenes as those studied in this paper but using colour negatives scanned at a much higher spatial resolution (see Fig. 7).

References

[1] J. Sanchiz, F. Pla, J.A. Marchant, R. Brivot, Structure from motion techniques applied to crop field imaging, Image and Vision Computing 14 (1996) 353–363.

[2] T. Hague, J.A. Marchant, N. Tillett, Autonomous robot navigation for precision horticulture, in: IEEE Int. Conf. on Robotics and Automation, Albuquerque, NM, April 1997, pp. 1880–1885.

[3] B. Southall, J.A. Marchant, T. Hague, B.F. Buxton, Model based tracking for navigation and segmentation, in: H. Burkhardt, B.B. Neumann (Eds.), Fifth European Conference on Computer Vision, Lecture Notes in Computer Science, 1406, Springer, Berlin, 1998, pp. 797–811.

[4] J.A. Marchant, R. Brivot, Real-time tracking of plant rows using a Hough transform, Real-Time Imaging 1 (1995) 363–371.

[5] R. Brivot, J.A. Marchant, Segmentation of plants and weeds for a precision crop protection robot using infrared images, IEE Proceedings: Vision, Image and Signal Processing 143 (2) (1996) 118–124.

[6] J.A. Marchant, R. Tillett, R. Brivot, Real-time segmentation of plants and weeds, Real-Time Imaging 4 (1998) 243–253.

[7] J. Serra, Image Analysis and Mathematical Morphology, Academic Press, London, 1982.

[8] J. Serra (Ed.), Theoretical Advances, Image Analysis and Mathematical Morphology, 2, Academic Press, London, 1988.

[9] H. Heijmans, Morphological Image operators, Advances in Electronics and Electron Physics, Academic Press, Boston, MA, 1994.

[10] P. Soille, Morphological Image Analysis, Springer, Berlin, 1999.

[11] B.F. Merembeck, B.J. Turner, Directed canonical analysis and the performance of classifiers under its associated linear transformation, Transactions on Geosciences and Remote Sensing, IEEE 18 (1980) 190–196.

[12] R. Gershon, A. Jepson, J. Tsotsos, Ambient illumination and the determination of material changes, Journal of the Optical Society of America A 3 (1986) 1700–1707.

[13] G. Klinker, A Physical Approach to Color Image Understanding, A.K. Peters Ltd, Wellesley MA, 1993.

[14] P. Soille, Morphological partitioning of multispectral images, Journal of Electronic Imaging 5 (3) (1996) 252–265.

[15] K. Fu, J. Mui, A survey on image segmentation, Pattern Recognition 13 (1981) 3–16.

[16] B. Schachter, L. Davis, A. Rosenfeld, Some experiments in image segmentation by clustering of local feature values, Pattern Recognition 11 (1) (1979) 19–28.

[17] M. Grimaud, New measure of contrast: dynamics, in: P. Gader, E. Dougherty, J. Serra (Eds.), Image Algebra and Morphological Image Processing III, SPIE-1769, July 1992, pp. 292–305.

[18] F. Feyaerts, P. Pollet, L. Van Gool, P. Wambacq, Vision system for automatic weed detection, in: P. Whelan (Ed.), Proc. Irish Machine Vision and Image Processing Conference, Irish Pattern Recognition Society, Dublin City University, 1999, pp. 288–299.

[19] G. Carter, Responses of leaf spectral reflectance to plant stress, American Journal of Botany 80 (3) (1993) 239–243.

[20] F. Meyer, Automatic screening of cytological specimens, Computer Vision, Graphics, and Image Processing 35 (1986) 356–369.

[21] C. Ronse, H. Heijmans, The algebraic basis of mathematical morphology II. Openings and closings, Computer Vision, Graphics, and Image Processing: Image Understanding 54 (1) (1990) 74–97.

[22] T. Huang, G. Yang, G. Tang, A fast two-dimensional median filtering algorithm, IEEE Transactions on Acoustics, Speech, and Signal Processing 27 (1) (1979) 13–18.

[23] B. Chaudhuri, An efficient algorithm for running window pel gray level ranking in 2-D images, Pattern Recognition Letters 11 (2) (1990) 77–80.

[24] F. Cheng, A. Venetsanopoulos, An adaptive morphological filter for image processing, IEEE Transactions on Image Processing 1 (4) (1992) 533–539.

[25] B. Southall, T. Hague, J.A. Marchant, B.F. Buxton, Vision-aided outdoor navigation of an autonomous horticultural vehicle, in: H. Christensen (Ed.), First International Conference on Computer Vision Systems, volume 1542 of Lecture Notes in Computer Science, Springer, Berlin, 1999, pp. 37–50.

[26] H.L. van Trees, Detection, Estimation, and Modulation Theory, 1, Wiley, New York, 1968.

[27] C. Shekhar, S. Moisan, R. Vincent, P. Burlina, R. Chellappa, Knowledge-based control of vision systems, Image and Vision Computing 17 (1999) 667–683.

[28] A. Sanchez, J.A. Marchant, Depth from motion applied to crop field imaging, Fusing 3D information for crops/weeds classification in: Fifteenth International Conference on Pattern Recognition, Barcelona, 2000, IEEE Computer Society, Los Alamito, California.